Inelastic Neutron Scattering Spectrum of $Cs_2[B_{12}H_{12}]$: Reproduction of Its Solid-State Vibrational Spectrum by Periodic DFT

Damian G. Allis and Bruce S. Hudson*

Department of Chemistry, 1-014 Center for Science and Technology, Syracuse University, Syracuse, New York 13244-4100

Received: September 17, 2005; In Final Form: December 28, 2005

The inelastic neutron scattering (INS) spectrum of polycrystalline $Cs_2[B_{12}H_{12}]$ is assigned through 1200 cm^{-1} on the basis of aqueous and solid-state Raman/IR measurements and normal mode analyses from solid-state density functional theory. The Cs^+ cations are responsible for frequency shifts of the internal cage vibrational modes and I_h cage mode splittings due to the crystal T_h site symmetry. These changes to the $[B_{12}H_{12}]^{2-}$ molecular modes make isolated-molecule calculations inadequate for use in complete assignments. Solid-state calculations reveal that 30/40 cm^{-1} shifts of T_g/H_g molecular modes are responsible for structure in the INS spectrum unobserved by optical methods or in aqueous solutions.

Introduction

The I_h symmetry *closo*-borane $[B_{12}H_{12}]^{2-}$ is a molecular cluster exhibiting aromatic three-dimensional electron delocalization and remarkable chemical stability.[1] The I_h symmetry predicted in theoretical studies and evident from spectroscopic studies is lost in the T_h site symmetry of the *closo*-$[B_{12}H_{12}]^{2-}$/group I salts, where T_h cage deformation is observed in the crystal structures of $M_2[B_{12}H_{12}]$ (M = K, Rb, or Cs; all cells $Fm\bar{3}$, $Z = 4$). In these crystal structures, the average skeletal B−B bond length differences with the softest (Cs^+, Δ_{B-B} = 0.001 Å)[2] and hardest (K^+, Δ_{B-B} = 0.005 Å)[3] cations are both small and similar, while this bond length difference in the reported crystal structure of the Rb^+ salt is unexpectedly large (and worth re-examination) at 0.134 Å.[4]

In a previous survey article,[5] it was shown that the inelastic neutron scattering (INS) spectrum of $Cs_2[B_{12}H_{12}]$, while otherwise in agreement with predictions based on the vibrations computed for an isolated dianion, differed considerably in the 900−1100 cm^{-1} region. All isolated dianion calculations yielded three features in this region of the spectrum where the INS experiment showed four. The INS spectrum could only be reproduced by the 50−70 cm^{-1} movements of calculated peaks from among a closely spaced set of four dianion modes with different symmetry. While the intensities computed for the INS transitions showed that rearrangements of the positions of peaks could result in a spectrum that agreed with experiment, molecular calculations could not be used to identify which modes required shifting or, in the T_h site symmetry of the crystal cell, both splitting and shifting. This large discrepancy between theory and experiment is rare in other cases except where strong intermolecular interactions due to hydrogen bonding occur. As the vibrations observed in IR and Raman spectra for the dianion in solution are in reasonable agreement with the results of calculations for the isolated cage, a theoretical treatment of the $Cs_2[B_{12}H_{12}]$ crystal cell is expected to elucidate the origin of the structure in the INS spectrum, be that structure due to simple shifts of I_h vibrations or large splittings due to the T_h site symmetry of the crystal cell.

* To whom correspondence should be addressed. Telephone: (315) 443-5805. Fax: (315) 443-4070. E-mail: bshudson@syr.edu.

This study utilizes optical (solution and solid-state) and theoretical (molecular and solid-state) methods to assign the INS spectrum of $Cs_2[B_{12}H_{12}]$ to 1200 cm^{-1}. The crystal cell differs from the isolated dianion by the presence of both cage-deforming packing interactions and counterions that affect the molecular normal modes through ionic interactions. These same two crystal features were considered separately in studies of the I_h hydrocarbon dodecahedrane ($I_h \rightarrow T_h$ site symmetry reduction and degenerate mode splittings)[6] and the Na^+ and K^+ salts of $[BH_4]^-$ (40−80 cm^{-1} shifts of molecular modes due to ionic interactions[7]). From the INS spectrum assignment and correlation of observed optical and neutron peaks, these two features of the crystal cell and the importance of the environment in instigating $[B_{12}H_{12}]^{2-}$ vibrational changes can be considered in detail.

Methods

The INS experiment was carried out using the TOSCA instrument at the ISIS facility of the Rutherford Appleton Laboratory, using approximately 1 g of polycrystalline $Cs_2[B_{12}H_{12}]$ held at 15 K. Details of the TOSCA spectrometer can be found elsewhere.[8] The room-temperature crystallographic data for $Cs_2[B_{12}H_{12}]$ are as follows: space group $Fm\bar{3}$ (face-centered cubic, "fcc"), $a = 11.281$ Å, $Z = 4$.[6] The INS spectrum measured at ISIS is available for download from the Database of Inelastic Neutron Scattering Spectra.[9]

Density functional theory (DFT) calculations were performed using Gaussian 03[10] and DMol^3.[11] Gaussian 03 was used for the geometry optimization and normal mode analysis of the isolated $[B_{12}H_{12}]^{2-}$ cage using the 6-31+G(d,p) Gaussian basis set,[12] the B3LYP hybrid density functional,[13] the program option "tight" convergence criteria, and an ultrafine grid size (corresponding to a grid of 99 radial shells and 590 angular points per shell), herein termed B3LYP. DMol^3 calculations were performed on the SGI Origin Array at the National Center for Supercomputing Applications (NCSA). DMol^3 does not allow for the optimization of lattice constants and uses average atomic masses as calculated from isotopic abundances. For both the isolated molecule and primitive cell ($k = 0$, $Z = 1$), the BOP generalized-gradient approximation density functional[14] and dnp numerical basis set[15] were used with the program option "fine"

10.1021/jp055285m CCC: $33.50
Published on Web 02/22/2006

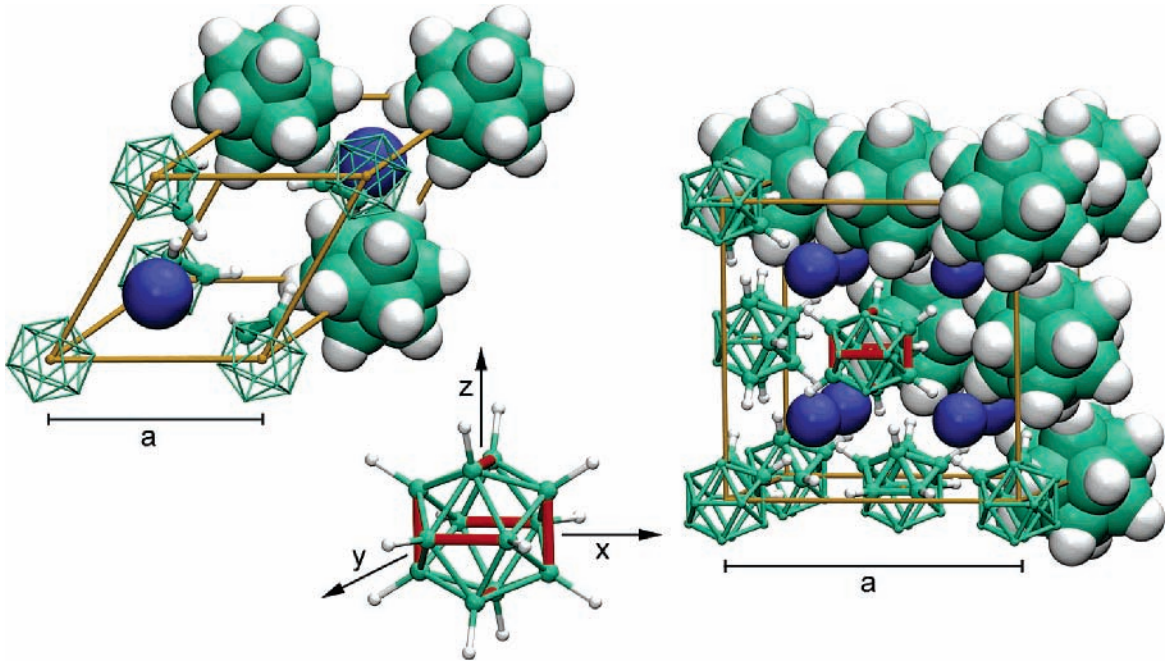

Figure 1. Primitive cell (left, $a = 7.977$ Å, $\alpha = 60°$) and $Fm\bar{3}$ fcc unit cell (right, $a = 11.281$ Å, $\alpha = 90°$) of $Cs_2[B_{12}H_{12}]$ (blue for Cs, green for B, and white for H) in mixed van der Waals and CPK representations. Also shown (in red) are the cage bond pairs along which $I_h \rightarrow T_h$ deformation occurs in the crystal cell (based on a cage extracted from the $Fm\bar{3}$ figure, the origin of the constituent axes being the cage center of mass). Images were rendered with VMD.[21]

TABLE 1: Crystallographic (Cs^+) and Calculated (isolated cage and solid-state) Bond Lengths and Atomic Distances in Angstroms[a]

		R_s	R_l	$R_l - R_s$	$(B-B)_{ave}$	B−H	M−B
isolated dianion	B3LYP				1.788_3	1.205_5	
	BOP				1.804_4	1.214_5	
solid-state DFT	BOP	1.781_8	1.788_4	0.006_6	1.787_1	1.200_2	3.682_6
experiment[2]	Cs^+	1.780	1.781	0.001	1.781	1.121	3.686

[a] Solid-state BOP/dnp calculations were performed on the basis of the Cs^+ salt crystal coordinates from ref 2.

grid size (*k*-point spacing of 0.04 $Å^{-1}$) and program option "fine" convergence criteria ($\Delta E < 1 \times 10^{-6}$ Hartree) for structure optimizations and normal mode analyses (herein termed BOP/dnp). Full fcc unit cell ($Z = 4$) and primitive unit cell ($Z = 1$) energy minimizations and normal mode analyses were also performed using the BOP functional and dn numerical basis set (BOP/dn). The lack of normal mode symmetry assignments in DMol[3] was reconciled with a simple g/u analysis performed by summation over the eigenvectors in each normal mode of inversion center-related atoms. Despite some small (up to 2 cm^{-1} [1]) variability among the degenerate modes calculated for the isolated $[B_{12}H_{12}]^{2-}$ in DMol[3], the selected convergence criteria were found to be adequate for analysis and symmetry assignment. Frequencies are reported as obtained from the calculations without scaling.

Results

$Cs_2[B_{12}H_{12}]$ Crystal and Calculated Structures. The $Fm\bar{3}$ fcc unit cell ($Z = 4$), the primitive cell ($Z = 1$), and the isolated $[B_{12}H_{12}]^{2-}$ cage are shown in Figure 1. Cage deformation in the room-temperature Cs^+ lattice is the smallest observed from among the series of characterized $[B_{12}H_{12}]^{2-}$ salts, with only a 0.001 Å difference between the six shortened (1.780 Å) and 24 elongated (1.781 Å) B−B bonds in the T_h site symmetry (Table 1). The X-ray value of the B−H bond lengths for the Cs^+ salt reflects the expected shortening due to the off-nuclear electron density.

Isolated dianion B3LYP and BOP/dnp cage bond lengths and relevant BOP/dnp crystal cell distances are provided in Table 1. The BOP/dnp bond lengths for the isolated cage are slightly longer (approximately 0.015 Å) than the bond lengths calculated at the B3LYP/6-31+G(d,p) (B−B, 1.788 Å), B3LYP/6-31G(d) (B−B, 1.787 Å),[16] and MP2/6-31G(d) (B−B, 1.782 Å)[17] levels of theory. The BOP/dnp primitive cell geometry optimization led to a 0.02 Å (average) reduction in B−B bond lengths relative to the isolated anion BOP/dnp bond lengths and differentiation of specific B−B bonds. The calculated average B−B bond length is 0.006 Å larger than the average cage bond length in the Cs^+ crystal cell. The primitive cell BOP/dnp difference between long and short B−B bonds [$R_l - R_s$] is 6−7 times larger than the reported deformation value (Table 1). This and the larger calculated average value of the B−B bond length are due primarily to the notably longer ($B-B_{large}$) distance. This structural deformation, associated with the change from I_h to T_h symmetry, results in splitting of the 4- and 5-fold degenerate modes, including H_g Raman active modes, and induction of intensity in otherwise inactive modes. The comparison of computed and observed spectral features permits a test of the validity of the computed deformation.

Spectroscopy. The molecular vibrational modes of the I_h $[B_{12}H_{12}]^{2-}$ cage split in the T_h site symmetry of the $Cs_2[B_{12}H_{12}]$ crystal cell as follows: $\mathbf{I_h}(T_h) \rightarrow \mathbf{2A_g}(2A_g) + \mathbf{T_{1g}}(T_g) + \mathbf{2G_g}$-$(2A_g + 2T_g) + \mathbf{4H_g}(4T_g + 4E_g) + \mathbf{3T_{1u}}(3T_u) + \mathbf{2T_{2u}}(2T_u) + \mathbf{2G_u}(2A_u + 2T_u) + \mathbf{2H_u}(2T_u + 2E_u)$. The IR and Raman spectra of various $[B_{12}H_{12}]^{2-}$ salts have been reported both as

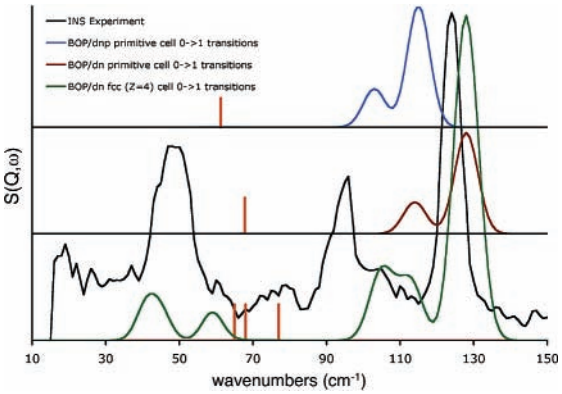

Figure 2. 10−150 cm^{-1} (phonon) region of the INS spectrum. The positions of the Cs^+ phonon modes in the calculations are shown as orange vertical bars.

aqueous solutions and in the solid state. Of relevance for the INS spectrum analysis are the aqueous spectra of the Na^+ and K^+ salts (for vibrational frequencies of the I_h symmetry cages)[18] and the solid-state IR and Raman spectra of the $Cs_2[B_{12}H_{12}]$ salt[19] (for vibrational frequencies of the T_h site symmetry cages of this salt). The room-temperature IR spectrum of the $Cs_2[B_{12}H_{12}]$ crystal provides excellent cage deformation detail of spectral changes in regions where the crystal T_h site symmetry yields IR activity with G_u and H_u cage (I_h) mode splittings. The INS analyses are divided into (1) the phonon region, (2) the low-frequency (400−1200 cm^{-1}) molecular vibrational region based on Raman, IR, B3LYP, and BOP/dnp results, and (3) the assignment of the 400−1200 cm^{-1} region based on a full theoretical overtone/combination band analysis using aCLIMAX.[20]

(1) Phonon Region (0−250 cm^{-1}). The simulated spectra for the BOP/dnp primitive cell, the BOP/dn primitive cell, and the BOP/dn fcc unit cell are provided with the INS spectrum in Figure 2. With two Cs^+ cations and a single cage in the primitive cell, the phonon modes divide into three triply degenerate mode groups corresponding to in-phase (same direction) Cs^+ cation motions, out-of-phase (opposite direction) Cs^+ cation motions, and three $[B_{12}H_{12}]^{2-}$ rotations (around *x*, *y*, or *z*). The BOP/dnp and BOP/dn primitive cell peak positions differ from one another by as much as 13 cm^{-1} [BOP/dnp and BOP/dn, 61.2 and 67.8 (T_g) cm^{-1}, 103.7 and 114.3 (T_u) cm^{-1}, and 115.9 and 128.1 (T_g) cm^{-1}, respectively], with these differences being attributable only to the choice of basis set. The primitive cell BOP/dnp phonon region is composed of three sets of triply degenerate modes, including out-of-phase cation modes (61.2 cm^{-1}), in-phase Cs^+/cage-coupled modes (103.7 cm^{-1}), and modes resulting from Cs−$[B_{12}H_{12}]$−Cs rocking motions/cage rotations in the primitive cell (115.9 cm^{-1}). The primitive cell modes at 103.7 and 115.9 cm^{-1} fall between the two major INS peaks at 96 and 124 cm^{-1}. The lack of hydrogen motion in the primitive cell 61.2 cm^{-1} modes argues against assignment to the major peak at 48 cm^{-1}, making it clear that only considering the primitive cell cannot account for many features in this region.

The phonon region gains appreciable structure in the full fcc ($Z = 4$) unit cell calculation due to the inclusion of out-of-phase ($k = \pi/a$) relative motions between neighboring primitive unit cells that cannot be calculated in the in-phase ($k = 0$) limit of the single primitive cell. The fcc BOP/dn calculation yields 15 triply degenerate modes grouped into six regions which account for the major features of the INS phonon spectrum. Four groups of modes centered at 43 [41.7 (T_g), 45.5 (T_g)] and 59 [59.0 (T_g), 59.1 (T_g)] cm^{-1} flank the major INS peak at 48 cm^{-1}, which itself includes a shoulder to lower frequency (45 cm^{-1}) and small cusps at 37 and 61 cm^{-1}. The INS splitting of the 96 and 105 cm^{-1} peaks is reproduced by two pairs of modes centered at 106 [104.0 (T_g), 107.6 (T_g)] and 113 [112.7 (T_g), 114.7 (T_u)] cm^{-1}. The highest-lying of these calculated mode groups, at 114.7 cm^{-1}, is IR-active as determined by eigenvector analysis. The prominent INS peak at 124 cm^{-1}, corresponding to Cs−$[B_{12}H_{12}]$−Cs rocking motions/$[B_{12}H_{12}]^{-2}$ twisting modes in the crystal lattice, is reproduced by four sets of modes centered at 128.5 cm^{-1} (127.4, 127.5, 128.7, and 130.1 cm^{-1}, all T_g modes). The only features not reproduced by intensity in the BOP/dn fcc cell calculations are the small group of INS peaks with intensities at 74, 76, and 80 cm^{-1}. The relative positions of these peaks are reproduced in the BOP/dn spectrum as Cs^+-only motions, with negligible (hydrogen-derived) intensities, at 65.4 (T_g), 68.1 (T_g), and 76.7 (T_g) cm^{-1}. The 65.4 cm^{-1} mode is determined, by eigenvector analysis, to be Raman-active, placing it in good agreement with the solid-state Raman measurement at 58/59 cm^{-1}.

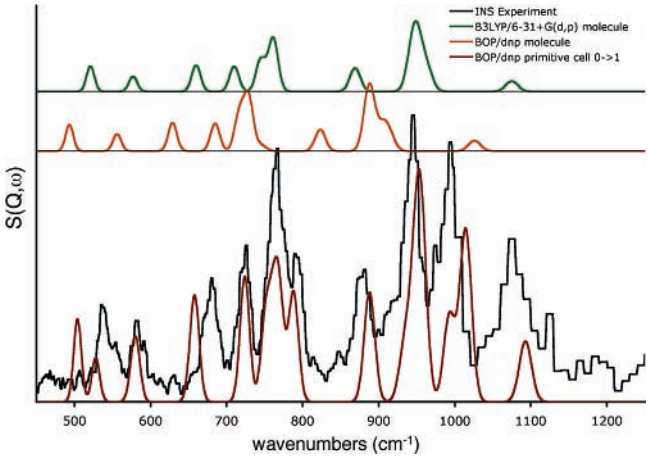

Figure 3. 500−1200 cm^{-1} INS spectrum and fundamental B3LYP/6-31+G(d,p), molecular BOP/dnp, and primitive cell BOP/dnp simulated spectra. The BOP/dnp primitive cell spectrum is superimposed on the INS spectrum for solid−solid spectral comparison.

(2) Low-Frequency Molecular Region (400−1200 cm^{-1}). The INS spectrum of $Cs_2[B_{12}H_{12}]$ from 400 to 1200 cm^{-1} is shown in Figure 3 and assigned to IR and Raman features in Table 2. Included in this table are the IR and Raman peaks from aqueous (Na^+ and K^+)[18] and solid-state $Cs_2[B_{12}H_{12}]$[19] measurements, and the isolated $[B_{12}H_{12}]^{2-}$ frequencies as determined from a B3LYP/6-31+G(d,p) normal mode analysis using the average boron mass of 10.811 amu. Included in Figure 3 are the simulated INS spectra for the isolated $[B_{12}H_{12}]^{2-}$ cage (B3LYP and BOP/dnp) and the primitive cell (BOP/dnp). The calculated frequencies at all presented levels of theory are provided with the INS peaks in Table 2. The assignments of INS features are presented below organized according to the B3LYP results for the I_h molecule.

522.0 cm^{-1} (H_u). These B3LYP modes occur in the INS spectrum as two features at 535.5 and 553 cm^{-1}. The isolated BOP/dnp calculations place these modes 30 cm^{-1} lower in frequency, while the primitive cell BOP/dnp calculations both shift and split the H_u modes into T_u (504 cm^{-1}) and E_u (529 cm^{-1}) components with calculated intensities consistent with the INS shape. The crystal splitting of the H_u mode into T_u and E_u components also gives rise to the IR-active T_u band in the solid state, unobserved in the aqueous studies, at 531 cm^{-1}.

577.7 cm^{-1} (H_g). These H_g modes appear as a single Raman peak in aqueous media (580−584 cm^{-1}, Table 2). The solid-state Raman spectrum contains two resolvable peaks of unequal

TABLE 2: INS, Raman and IR (aqueous[18] and solid-state[19]), and B3LYP/6-31+G(d,p) and BOP/dnp Vibrational Frequencies and (B3LYP) Symmetry Assignments for the I_h Point Group and T_h Crystal Site Symmetry[a]

	Raman		IR				
INS	aqueous $Na^+/K^+/K^+$	crystal Cs^+	aqueous Na^+/K^+	crystal Cs^+	B[10,811] B3LYP 6-31+G(d,p)	BOP/dnp isolated	BOP/dnp primitive
535.5				531 [T_u]	522.0 (H_u)	493.6 (H_u)	504.1 (T_u)
(553)							528.6 (E_u)
582	584/582/580	581 [T_g, E_g]			577.7 (H_g)	556.3 (H_g)	577.3 (E_g)
(592)		586 [T_g, E_g]					582.5 (T_g)
(632)					660.1 (G_g)	629.2 (G_g)	655.8 (A_g)
681							659.7 (T_g)
727			720/719 [T_u]	708/718 [T_u]	710.1 (T_{1u})	685.5 (T_{1u})	724.5 (T_u)
					744.7 (A_g)	734.9 (A_g)	753.9 (A_g)
	743/746/745	747 [A_g]			745.5 (G_u)	716.9 (G_u)	751.3 (T_u)
							759.7 (A_u)
768	770/774/770	762 [T_g, E_g]			761.1 (H_g)	729.1 (H_g)	762.2 (T_g)
		787 [T_g, E_g]					769.5 (E_g)
(790)				757 [T_u]	764.5 (T_{2u})	746.5 (T_{2u})	788.6 (T_u)
(848)				860 [T_u]	870.0 (G_u)	823.5 (G_u)	888.2 (T_u)
883							933.8 (A_u)
		940			943.2 (G_g)	886.3 (G_g)	941.8 (A_g)
							950.9 (T_g)
946					949.1 (H_u)	889.9 (H_u)	953.7 (E_u)
	949/954/955			950 [T_u]			957.3 (T_u)
(975)		972			954.5 (H_g)	914.7 (H_g)	1014.0 (T_g)
995							1015.8 (E_g)
					964.1 (T_{1g})	905.2 (T_{1g})	993.5 (T_g)
1076			1070/1071 [T_u]	1057, 1073 [T_u]	1075.4 (T_{1u})	1026.5 (T_{1u})	1093.1 (T_u)

[a] Closely spaced minor peaks in the INS spectrum are in parentheses.

height at 581 (major) and 586 (minor) cm^{-1}, consistent in position and relative splitting with the two resolvable INS peaks at 582 (major) and 592 (minor) cm^{-1}, respectively. These H_g molecular BOP/dnp modes shift 15 cm^{-1} to higher frequencies in the solid-state calculation and split into T_g (lower) and E_g (higher) components with a 5 cm^{-1} separation. The presence of two peaks in the solid-state calculations is consistent with T_h site symmetry splitting of these H_g modes.

660.1 cm^{-1} (G_g). These G_g modes are unobserved in the aqueous and solid-state optical studies. The corresponding INS peak (681 cm^{-1}) is flanked by small features at 624 and 698 cm^{-1}, both shown in the aCLIMAX analysis to be combination bands. The INS peak itself shows little structure, while the BOP/dnp solid-state calculation predicts a 4 cm^{-1} splitting of the G_g mode into T_g and A_g components (Table 3), both of which are formally Raman-allowed but, again, are unobserved in the solid-state Raman study.

710.1 cm^{-1} (T_{1u}). The IR-active T_{1u} modes in the I_h point group are of T_u symmetry in T_h and, therefore, are unsplit and IR-active in the crystal cell. The molecular BOP/dnp frequencies for these modes shift 39 cm^{-1} to higher frequencies in the solid state to yield good agreement with both INS and IR peak positions. While the INS peak is devoid of other features, the IR spectrum of the crystal yields two resolvable peaks of nearly equal height at 708 and 718 cm^{-1} (Table 2).

744.7 (A_g), 745.5 (G_u), 761.1 (H_g), and 764.5 (T_{2u}) cm^{-1}. These modes are responsible for a large INS feature with a maximum at 768 cm^{-1} and a smaller, though very prominent, peak at 790 cm^{-1} (Figure 3). This narrow region also contains the highest concentration of Raman and IR structure, which is key to testing the theoretical results in the absence of resolved INS data. The only measured IR vibration in this region occurs in the crystal at 757 cm^{-1}. The Raman spectrum of the crystal can be divided into three peaks at 747, 762, and 787 cm^{-1}. The aqueous Raman peaks occur at 743/745 and 770/774 cm^{-1}. From polarized Raman studies, it is known that the most prominent peak in this region (747 cm^{-1}) is the totally symmetric A_g skeletal B−B mode, assigned to the BOP/dnp A_g mode at 754 cm^{-1}. The small size of this peak in the INS spectrum can be attributed to the localization of this skeletal mode to the B−B bonds and not to hydrogen atoms, whose motions are responsible for INS intensity. The 757 cm^{-1} IR peak is consistent in position with the T_u components (751 cm^{-1}) of the G_u modes as split in the crystal cell. The T_h-split BOP/dnp (solid-state) H_g modes at 762 (T_g) and 770 (E_g) cm^{-1} are the only modes whose symmetry yields Raman activity in this region, placing their assignments at the higher-frequency crystal Raman modes of 762 and 787 cm^{-1}. By comparing the INS spectrum with the BOP/dnp primitive cell calculations, we found that the T_{2u} mode entirely accounts for the INS peak at 790 cm^{-1}, leaving the remaining three I_h (A_g, G_u, and H_g) mode groups (which occur as five distinct mode groups in the T_h site symmetry) to account for the size and broadness of the 768 cm^{-1} INS peak.

870.0 cm^{-1} (G_u). These G_u modes are significantly shifted from their BOP/dnp molecular frequency (823 cm^{-1}) and split by 46 cm^{-1} in the BOP/dnp primitive cell into T_u (888 cm^{-1}) and A_u (934 cm^{-1}) components. The IR-active T_u modes occur in the solid-state IR spectrum at 860 cm^{-1}, while the major INS feature in this region occurs with only a single peak at 883 cm^{-1}. The A_u component (934 cm^{-1}) is shifted into the low-frequency region of the next larger INS feature.

943.2 (G_g), 949.1 (H_u), 954.5 (H_g), and 964.1 (T_{1g}) cm^{-1}. These modes are responsible for the most interesting features in the INS spectrum, as their narrow B3LYP separation is inconsistent with the two large INS features occurring in the 950−1000 cm^{-1} region. Only the B3LYP H_u mode at 949 cm^{-1} contains any component that can become IR-active in the T_h site symmetry, leaving the crystal IR peak at 950 cm^{-1} to be assigned to the BOP/dnp T_u modes at 957 cm^{-1}. The highest-frequency solid-state Raman mode observed at 972 cm^{-1} is in good agreement with the INS peak at 975 cm^{-1} while lying below a single calculated T_g mode at 994 cm^{-1} and a closely spaced pair of H_g-derived E_g/T_g modes at 1015 cm^{-1}. The INS

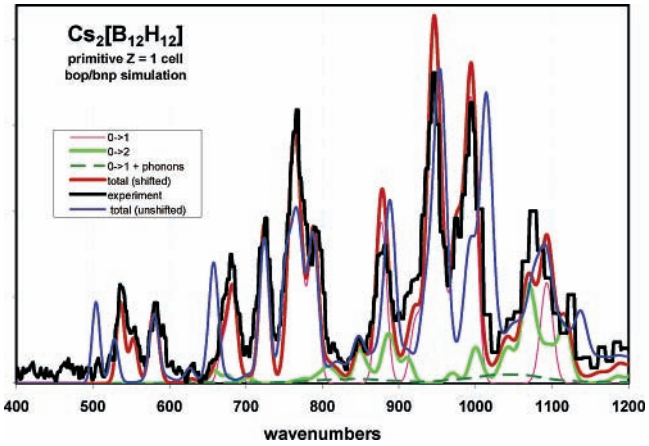

Figure 4. 400−1200 cm^{-1} INS spectrum with both the BOP/dnp primitive cell simulated spectrum (blue) and the INS-corrected (mode-shifted) BOP/dnp spectrum (red). Included in this figure are the component fundamental (pink), two-quantum (green), and fundamental and INS phonon (dashed dark green) spectra. In converting the computed spectrum (blue trace) to the "shifted" red trace, we applied the following transition shifts: 505 cm^{-1} → 536 cm^{-1}, 521 cm^{-1} → 553 cm^{-1}, 654.6 cm^{-1} → 680 cm^{-1}, 781 cm^{-1} → 766 cm^{-1}, 871 cm^{-1} → 880 cm^{-1}, 993.5 cm^{-1} → 975 cm^{-1}, 1014.0 cm^{-1} → 993 cm^{-1}, 1015.8 cm^{-1} → 995 cm^{-1}.

spectrum contains a large peak at 995 cm^{-1} that the Raman spectrum does not. By inspection of the intensities of the INS and BOP/dnp spectra, the B3LYP T_g mode at 964 cm^{-1} is likely the origin of the INS/Raman peaks at 975/972 cm^{-1} and is therefore assigned to the BOP/dnp primitive cell peak at 994 cm^{-1}. This assignment leaves the B3LYP H_g modes at 954.5 cm^{-1} to account for the INS peak at 995 cm^{-1}, 20 cm^{-1} lower than the BOP/dnp primitive cell peaks at 1015 cm^{-1}. These assignments of the calculated results leave the G_g (943 cm^{-1}) and H_u (949 cm^{-1}) modes responsible for the INS peak with a strong maximum at 946 cm^{-1}.

1075.4 cm^{-1} (T_{1u}). While the last of the low-frequency molecular modes occurs sufficiently high above the previous region to allow for its unencumbered assignment, this region of the INS spectrum contains additional features that can only be attributed to combination bands (see below). The B3LYP T_{1u} mode is T_u in the T_h point group and is, therefore, IR-active, occurring in both aqueous and solid-state studies. The Cs^+ crystal IR spectrum contains three peaks at 1057, 1073 (both of nearly equal intensity), and 1116 cm^{-1} (small but resolvable). This region of the INS spectrum is dominated by one broad peak centered at 1079 cm^{-1} and a distinct peak to a higher frequency at 1131 cm^{-1}. As the T_{1u} mode in I_h symmetry is unsplit in the T_h site symmetry, the calculated frequencies can be assigned to only one of the features in this region. The proximity and separation of the IR data relative to the other peaks in this region indicate that the 1076 cm^{-1} INS feature is due to the calculated T_u mode in the solid state at 1093 cm^{-1} (BOP/dnp).

(3) Overtone and Combination Contributions. The intensities of *n*-quantum transitions in INS spectroscopy scale by the square of the *n*th power of the momentum transfer, *Q*. For the TOSCA spectrometer, *Q* increases with transition energy. Multiquantum transitions thus become both more numerous and more intense at higher frequencies.

In Figure 4, the dashed green trace shows the sum of all contributions as computed directly from the primitive cell BOP/dnp calculation but with addition of the first 75 cm^{-1} of the experimental spectrum so as to include the phonon "wing" contributions in this "molecular fundamental" region (0 → 1 + phonon). The major contributions from the combinations and overtones occur in the higher-energy region of this spectrum. There are several features in the calculated spectrum that clearly correspond to nearby features of the experiment. Significant discrepancies between the fundamental BOP/dnp and INS spectra can be removed by changing the calculated frequencies of a few bands slightly so that they agree with the major INS features assigned in the fundamental mode analysis. The specific adjustments are given in the figure legend. The result of these corrections to the overall spectrum is shown in red in Figure 4. These shifts have the general effect of "compressing" the spectrum. The binary overtones and combinations that contribute in this region are colored green with the darker dashed green line being the phonon wings added to the fundamental transitions. These are computed using the shifted fundamentals. There are a few small features (e.g., at 849 cm^{-1}; compare with Figure 3) that are due entirely to combinations. In the region above 1030 cm^{-1}, the overtone and combination intensity exceeds that of the fundamental transitions.

Discussion

This solid-state DFT study of $Cs_2[B_{12}H_{12}]$ was motivated by disagreement between the normal mode analysis of the isolated (I_h symmetry) B3LYP/6-31G(d,p) cage and the observed $Cs_2[B_{12}H_{12}]$ INS spectrum.[5] Isolated-molecule calculations ascribe the 883 cm^{-1} INS peak to a G_u mode, leaving a large composite feature from 900 to 1125 cm^{-1} for which four molecular modes of G_g, H_g, H_u, and T_{1g} symmetries can account. Isolated molecule calculations group all four of these modes into a narrow (20 cm^{-1}) region (see Table 3), so all appear as a single peak when simulated with appropriate bandwidths. The correct groupings of these molecular modes as observed features occur in the unit cell treatment of vibrational shifting and splitting as follows. The three features in this region at 883, 946, and 995 cm^{-1} are found to originate from all five of the aforementioned molecular modes: G_u plus [G_g,H_g,H_u,T_{1g}]. The G and H modes are all split in the lower T_h crystal symmetry. The INS peak at 883 cm^{-1} is entirely composed of the T_u component of the G_u molecular mode. The INS peak at 946 cm^{-1} is composed of the remaining A_u crystal mode of the molecular G_u group plus the G_g and H_u modes (all components), with the H_u modes responsible for both the observed INS and IR intensity in the 950 cm^{-1} region. The INS peak at 995 cm^{-1} and the smaller feature at 975 cm^{-1} are composed of the summation of the contributions of the components of the H_g (995 cm^{-1}) and T_{1g} (975 cm^{-1}) molecular modes. The slight splitting of this H_g/T_{1g} grouping can, given the relative intensities of the H_g and T_{1g} peaks, be assigned to the T_g unaffected by the T_h crystal environment. The major effect of the crystal field in the INS spectrum is to differentially shift the (I_h) H_g mode group, at 954 cm^{-1}, 40 cm^{-1} to a higher frequency while leaving many of the remainder of the calculated modes unchanged.

Conclusions

The INS spectrum of $Cs_2[B_{12}H_{12}]$ has been assigned on the basis of the results of optical studies and solid-state DFT calculations. Splittings of degenerate modes due to the T_h site symmetry of the crystal cell are present to varying degrees in the optical studies and are very clear in the isolated/solid-state DFT analysis. Both the major discrepancy between the isolated molecule and INS spectra (900−1100 cm^{-1} region) and much of the additional structure in the INS spectrum due to overtone/combination features are correctly assigned in the solid-state DFT analysis. The importance of considering both frequency

and intensity/H-atom motions in the solid-state DFT calculations is demonstrated in the Cs^+ phonon modes that are visible in the INS spectrum and, importantly, whose frequencies are accurately predicted. The assignment of additional vibrational structure in the INS spectrum by way of overtone/combination inclusion in the solid-state DFT analysis demonstrates both the importance of multiquantum transitions in INS spectroscopy and the need to consider these transitions as part of theoretical analyses in accurately reproducing and assigning INS spectra. The computed structure for the $[B_{12}H_{12}]^{2-}$ cage using the reported crystallographic unit cell parameter results in a cage ($\Delta R \cong 0.0066$ Å) more deformed than that reported for the analysis of the diffraction data ($\Delta R \cong 0.001$ Å). If this structural deformation vanishes, the observed and computed splitting values also vanish. Given the generally good agreement between the computed and observed 15 K INS spectral splitting for the H_g, H_u, and G_u modes, the computed structure appears to be much closer to that present in the cesium salt crystal at low temperatures than that reported in the room-temperature X-ray study.

Acknowledgment. The Rutherford Appleton Laboratory is thanked for neutron beam access at the ISIS facility where the TOSCA spectrometer was used. The National Center for Supercomputing Applications (University of Illinois, Urbana, IL) is thanked for access to the SGI Origin Array for the DMol^3 calculations. This work was supported by National Science Foundation Grant CHE 0240104 and by U.S. Department of Energy Grant DE-FG02-01ER14245.

References and Notes

(1) Schleyer, P. v. R.; Subramanian, G.; Jiao, H.; Najafian, K.; Hofmann, K. M. In *Advances in Boron Chemistry*; Siebert, W., Ed.; The Royal Society of Chemistry: Cambridge, England, 1997.

(2) Tiritiris, I.; Schleid, T.; Müller, K.; Preetz, W. *Z. Anorg. Allg. Chem.* **2000**, *626*, 323.

(3) Wunderlich, J. A.; Lipscomb, W. N. *J. Am. Chem. Soc.* **1960**, *82*, 4427.

(4) Uspenskaya, S. I.; Solntsev, K. A.; Kuznetsov, N. T. *Zh. Strukt. Khim.* **1975**, *16*, 482.

(5) Hudson, B. S. *J. Phys. Chem. A* **2001**, *105*, 3949.

(6) Hudson, B. S.; Allis, D. G.; Parker, S. F.; Ramirez-Cuesta, A. J.; Herman, H.; Prinzbach, H. *J. Phys. Chem. A* **2005**, *109*, 3418.

(7) Allis, D. G.; Hudson, B. S. *Chem. Phys. Lett.* **2004**, *385*, 166.

(8) Parker, S. F. *J. Neutron Res.* **2002**, *10*, 173.

(9) The Database of Inelastic Neutron Scattering Spectra is available at http://www.isis.rl.ac.uk/molecularspectroscopy/index.htm.

(10) Frisch, M. J.; Trucks, G. W.; Schlegel, H. B.; Scuseria, G. E.; Robb, M. A.; Cheeseman, J. R.; Montgomery, J. A., Jr.; Vreven, T.; Kudin, K. N.; Burant, J. C.; Millam, J. M.; Iyengar, S. S.; Tomasi, J.; Barone, V.; Mennucci, B.; Cossi, M.; Scalmani, G.; Rega, N.; Petersson, G. A.; Nakatsuji, H.; Hada, M.; Ehara, M.; Toyota, K.; Fukuda, R.; Hasegawa, J.; Ishida, M.; Nakajima, T.; Honda, Y.; Kitao, O.; Nakai, H.; Klene, M.; Li, X.; Knox, J. E.; Hratchian, H. P.; Cross, J. B.; Bakken, V.; Adamo, C.; Jaramillo, J.; Gomperts, R.; Stratmann, R. E.; Yazyev, O.; Austin, A. J.; Cammi, R.; Pomelli, C.; Ochterski, J. W.; Ayala, P. Y.; Morokuma, K.; Voth, G. A.; Salvador, P.; Dannenberg, J. J.; Zakrzewski, V. G.; Dapprich, S.; Daniels, A. D.; Strain, M. C.; Farkas, O.; Malick, D. K.; Rabuck, A. D.; Raghavachari, K.; Foresman, J. B.; Ortiz, J. V.; Cui, Q.; Baboul, A. G.; Clifford, S.; Cioslowski, J.; Stefanov, B. B.; Liu, G.; Liashenko, A.; Piskorz, P.; Komaromi, I.; Martin, R. L.; Fox, D. J.; Keith, T.; Al-Laham, M. A.; Peng, C. Y.; Nanayakkara, A.; Challacombe, M.; Gill, P. M. W.; Johnson, B.; Chen, W.; Wong, M. W.; Gonzalez, C.; Pople, J. A. *Gaussian 03*, revision B03; Gaussian, Inc.: Wallingford, CT, 2004.

(11) *DMol*^{3}; Accelrys: San Diego (http://www.accelrys.com). Delley, B. *J. Chem. Phys.* **2000**, *113*, 7756.

(12) Hydrogen: Hehre, W. J.; Ditchfield, R.; Pople, J. A. *J. Chem. Phys.* **1972**, *56*, 2257. Boron: Dill, J. D.; Pople, J. A. *J. Chem. Phys.* **1975**, *62*, 2921.

(13) The B3LYP functional is Becke's three-parameter hybrid method with the LYP correlation functional: Becke, A. D. *J. Chem. Phys.* **1993**, *98*, 5648.

(14) The BOP functional is Becke's one-parameter exchange functional (Becke, A. D. *Phys. Rev. A* **1988**, *38*, 3098) and one-parameter progressive correlation functional (Tsuneda, T.; Suzumura, T.; Hirao, K. *J. Chem. Phys.* **1999**, *110*, 10664).

(15) Delley, B. *J. Chem. Phys*. **1990**, *92*, 508.

(16) Schleyer, P. v. R.; Najafian, K.; Mebel, A. M. *Inorg. Chem.* **1998**, *37*, 6765.

(17) Schleyer, P. v. R.; Najafian, K. *Inorg. Chem.* **1998**, *37*, 3454.

(18) Leites, L. A.; Bukalov, S. S.; Kurbakova, A. P.; Kaganski, M. M.; Gaft, Yu. L.; Kuznetsov, N. T.; Zakharova, I. A. *Spectrochim. Acta* **1982**, *38A*, 1047.

(19) Srebny, H.-G.; Preetz, W.; Marsmann, H. C. *Z. Naturforsch.* **1984**, *39b*, 189.

(20) Ramirez-Cuesta, A. J. *Comput. Phys. Commun.* **2004**, *157*, 226.

(21) Humphrey, W.; Dalke, A.; Schulten, K. *J. Mol. Graphics* **1996**, *14*, 33.